Quantitative Proteomics with siRNA Screening Identifies Novel Mechanisms of Trastuzumab Resistance in HER2 Amplified Breast Cancers*[S]

Alaina P. Boyer‡§, Timothy S. Collier‡§, Ilan Vidavsky¶, and Ron Bose‡‖**

HER2 is a receptor tyrosine kinase that is overexpressed in 20% to 30% of human breast cancers and which affects patient prognosis and survival. Treatment of HER2-positive breast cancer with the monoclonal antibody trastuzumab (Herceptin) has improved patient survival, but the development of trastuzumab resistance is a major medical problem. Many of the known mechanisms of trastuzumab resistance cause changes in protein phosphorylation patterns, and therefore quantitative proteomics was used to examine phosphotyrosine signaling networks in trastuzumab-resistant cells. The model system used in this study was two pairs of trastuzumab-sensitive and -resistant breast cancer cell lines. Using stable isotope labeling, phosphotyrosine immunoprecipitations, and online TiO_2 chromatography utilizing a dual trap configuration, ~1700 proteins were quantified. Comparing quantified proteins between the two cell line pairs showed only a small number of common protein ratio changes, demonstrating heterogeneity in phosphotyrosine signaling networks across different trastuzumab-resistant cancers. Proteins showing significant increases in resistant *versus* sensitive cells were subjected to a focused siRNA screen to evaluate their functional relevance to trastuzumab resistance. The screen revealed proteins related to the Src kinase pathway, such as CDCP1/Trask, embryonal Fyn substrate, and Paxillin. We also identify several novel proteins that increased trastuzumab sensitivity in resistant cells when targeted by siRNAs, including FAM83A and MAPK1. These proteins may present targets for the development of clinical diagnostics or therapeutic strategies to guide the treatment of HER2+ breast cancer patients who develop trastuzumab resistance. ***Molecular & Cellular Proteomics 12: 10.1074/mcp.M112.020115, 180–193, 2013.***

HER2 is a member of the epidermal growth factor receptor (EGFR)/ErbB family of receptor tyrosine kinases. Under normal physiologic conditions, HER2 tyrosine kinase signaling is tightly regulated spatially and temporally by the requirement for it to heterodimerize with a ligand bound family member, such as EGFR, HER3/ErbB3, or HER4/ErbB4 (1). However, in 20% to 30% of human breast cancer cases, HER2 gene amplification is present, resulting in a high level of HER2 protein overexpression and unregulated, constitutive HER2 tyrosine kinase signaling (2, 3). HER2 gene amplified breast cancer, also termed HER2-positive breast cancer, carries a poor prognosis, but the development of the HER2 targeted monoclonal antibody trastuzumab (Herceptin) has significantly improved patient survival (2). Despite the clinical effectiveness of trastuzumab, the development of drug resistance significantly increases the risk of patient death. This poses a major medical problem, as most metastatic HER2-positive breast cancer patients develop trastuzumab resistance over the course of their cancer treatment (4). The treatment approach for HER2+ breast cancer patients after trastuzumab resistance develops is mostly a trial-and-error process that subjects the patient to increased toxicity. Therefore, there is a substantial medical need for strategies to overcome trastuzumab resistance.

Multiple trastuzumab-resistance mechanisms have been identified, and they alter signaling networks and protein phosphorylation patterns in either a direct or an indirect manner. These mechanisms can be grouped into three categories. The first category is the activation of a parallel signaling network by other tyrosine kinases. These kinases include the receptor tyrosine kinases, EGFR, IGF1R, Her3, Met, EphA2, and Axl, as well as the erythropoietin-receptor-mediated activation of the cytoplasmic tyrosine kinases Jak2 and Src (5–11). The second category is the activation of downstream signaling proteins. Multiple studies have demonstrated activation of the phosphatidylinositol-3-kinase (PI3K)/AKT pathway in trastuzumab resistance, which occurs either via deletion of the PTEN lipid phosphatase or mutation of the PI3K genes (12, 13). Activation of Src family kinases or overexpression of cyclin E, which increases the cyclin E–cyclin-dependent kinase 2 signaling pathway, has also been reported (14). The third category includes mechanisms that maintain HER2 signaling even in the presence of trastuzumab. The production of a truncated isoform of HER2, p95HER2, which lacks the trastuzumab binding site, causes constitutive HER2 signaling (15, 16). Overexpression of the MUC4 sialomucin complex inhibits

From the ‡Division of Oncology, Department of Medicine, Washington University School of Medicine, St. Louis, MO 63110; ‖Department of Cell Biology and Physiology, Washington University School of Medicine, St. Louis, MO 63110; and ¶Department of Chemistry, Washington University, St. Louis, MO 63130

Received April 27, 2012, and in revised form, September 18, 2012
Published, MCP Papers in Press, October 25, 2012, DOI 10.1074/mcp.M112.020115

trastuzumab binding to HER2 and thereby maintains HER2 signaling (17, 18).

Given that multiple trastuzumab-resistance mechanisms alter signaling networks and protein phosphorylation patterns, we reasoned that mapping phosphotyrosine signaling networks using quantitative proteomics would be a highly useful strategy for analyzing known mechanisms and identifying novel mechanisms of trastuzumab resistance. Quantitative proteomics and phosphotyrosine enrichment approaches have been extensively used to study the EGFR signal networks (19–23). We and others have used these approaches to map the HER2 signaling network (22, 24, 25). Multiple other tyrosine kinase signaling networks were analyzed using quantitative proteomics, including Ephrin receptor, EphB2 (26–28), platelet-derived growth factor receptor (PDGFR) (21), insulin receptor (29, 30), and the receptor for hepatocyte growth factor, c-MET (31).

The goal of this study is to identify, quantify, and functionally screen proteins that might be involved in trastuzumab resistance. We used two pairs of HER2 gene amplified trastuzumab-sensitive (parental, SkBr3 and BT474) and -resistant ($SkBr3^R$ and $BT474^R$) human breast cancer cell lines as models for trastuzumab resistance. These cell lines and their trastuzumab-resistant derivatives have been extensively characterized and highly cited in the breast cancer literature (32, 33). Using stable isotope labeling of amino acids in cell culture (SILAC),[1] phosphotyrosine immunoprecipitations, and online TiO_2 chromatography with dual trap configuration, we quantified the changes in phosphotyrosine containing proteins and interactors between trastuzumab-sensitive and -resistant cells. Several of the known trastuzumab-resistance mechanisms were identified, which serves as a positive control and validation of our approach, and large protein ratio changes were measured in proteins that had not been previously connected with trastuzumab resistance. We then performed a focused siRNA screen targeting the proteins with significantly increased protein ratios. This screen functionally tested the role of the identified proteins and identifies which proteins might have the largest effect on reversing trastuzumab resistance.

EXPERIMENTAL PROCEDURES

Cell Lines and Lysate Preparation—The trastuzumab-sensitive (SkBr3 and BT474, parental) and -resistant ($SkBr3^R$ and $BT474^R$) cells were derived and graciously given by the laboratory of Dr. Dennis Slamon (University of California at Los Angeles) (32). Cells were cultured in RPMI media (Invitrogen, Carlsbad, CA) supplemented with 10% fetal bovine serum (Sigma Aldrich, St. Louis, MO) and 1% Pen/Strep. SILAC labeling and culturing was performed as described elsewhere (34). Briefly, SILAC medium consisted of RPMI 1640 medium with 25 mM HEPES, 4 mM L-Glutamine without L-Arginine and L-Lysine (ThermoScientific, Rockford, IL). Light medium was supplemented with 10% dialyzed fetal bovine serum (Invitrogen), 0.27 mM L-lysine, and 0.58 mM L-arginine (Sigma Aldrich). Heavy medium was supplemented with 10% dialyzed fetal bovine serum, 0.27 mM $^{13}C_6$-L-lysine (Cambridge Isotope Laboratories, Andover, MA), and 0.58 mM $^{13}C_6$-L-arginine (Isotec, Miamisburg, OH). After four passages (roughly eight cell divisions) of cell expansion, the cells were washed twice in PBS and scraped and collected using modified radioimmune precipitation assay buffer (150 mM NaCl, 50 mM Tris-HCl, pH 7.4, 1% Nonidet P-40, 0.25% Sodium Deoxycholate, and 1 mM EDTA) containing phosphatase and protease inhibitors (PPI) (5 mM NaF, 5 mM β-Glycerophosphate, 1 tablet inhibitor mixture (Roche, Indianapolis, IN), and 1 mM activated sodium orthovanadate). Two replicate SILAC labeling experiments were performed on each cell line, differing only in the reversal of light and heavy isotope labels in the second replicate experiment (Fig. 1*C*). Eight milligrams of total cell lysate from the $SkBr3/SkBr3^R$ pair and 14 mg of total cell lysates from the $BT474/BT474^R$ pair were collected separately. Heavy and light isotope labeled samples were combined at a 1:1 ratio based on the total protein concentration as determined via Bradford assay. Immunoprecipitation was performed as follows: the whole cell lysate was pre-cleared using protein A/G agarose (Pierce, Rockford, IL) for 4 h. After preclearing, the lysate samples were centrifuged at 4000 rpm for 2 min at 4 °C, and the supernatant was collected. The supernatant was diluted to 40 ml using modified radioimmune precipitation assay lysis buffer supplemented with PPI, and 400 to 800 μl of two anti-phosphotyrosine antibodies were added to the lysates (equimolar amounts of immobilized phosphotyrosine, P-Tyr-100 (Cell Signaling Technologies, Danvers, MA), and anti-phosphotyrosine, clone 4G10, agarose conjugate (Millipore, Billerica, MA) were used) and incubated overnight, rotating at 4 °C. Supernatant was collected and stored at −80 °C for future use, and the agarose bead pellet was washed three times in radioimmune precipitation assay buffer with PPI. Two consecutive phenyl phosphate elutions (100 mM, ~500 μl each time) (Sigma Aldrich) were performed to collect the phosphoenriched fraction from the agarose beads for each pair of cell lines. Ten microliters from each ~500-μl elution fraction were collected for protein quantification and Western blot analysis. The eluate was precipitated in cold acetone at four times the sample volume overnight at −20 °C. Samples were centrifuged at 13,000 rpm for 10 min at 4 °C, acetone was discarded, and the pellet was dried and stored at −80 °C.

Sample Preparation for LC-MS/MS—215 μg (determined via Bradford assay) of phosphoenriched immunoprecipitated pellet from the $SkBr3/SkBr3^R$ and 312 μg from $BT474/BT474^R$ cells were brought to room temperature and resuspended in 8 M urea. Samples were reduced in 10 mM dithiothreitol (Sigma Aldrich) for 1 h at 57 °C and alkylated in 55 mM iodoacetamide (Sigma Aldrich) for 1 h in the dark at room temperature. The urea in the samples was diluted to less than 2 M with 100 mM ammonium bicarbonate, pH 7.5. Samples were digested with mass spectrometry grade trypsin (Promega, Madison, WI), at a ratio of 1:50 enzyme to substrate, overnight at 37 °C. The trypsin digestion was halted with the addition of formic acid (Sigma Aldrich) to a pH < 3 and desalted using PepClean C18 spin columns (Pierce). Desalted peptides were fractionated using the OFFGEL isoelectric focusing apparatus (Agilent Technologies, Santa Clara, CA) across a pH gradient from 3 to 10 according to the manufacturer's protocol. Twelve fractions were collected and desalted using PepClean C18 spin columns, dried, and stored at −20 °C until needed for mass spectrometric analysis.

Online TiO_2 Phosphopeptide Trapping and Reversed Phase LC—All LC solvents were purchased from Sigma Aldrich (St. Louis, MO). Dried peptide samples were reconstituted in 20 μl of 0.1% formic acid in MS grade water (Pierce). Nano-flow chromatography was per-

[1] The abbreviations used are: ER, estrogen receptor; IP, immunoprecipitation; PANTHER, Protein Analysis through Evolutionary Relationships; PPI, phosphatase and protease inhibitors; PR, progesterone receptor; pTyr, phosphotyrosine; SILAC, stable isotope labeling by amino acids in cell culture; siRNA, short interfering RNA.

formed on an UltiMate 3000 RSLCnano (Dionex, Sunnyvale, CA) utilizing a dual-trap configuration on two six-port valves in series with an analytical reversed phase column. 5 μl of sample was loaded onto the traps with a loading solvent consisting of 0.05% heptafluorobutyric acid (HFBA) in water onto a TiO_2 trap (200 μm inner diameter $\times$ 1 cm, 5 μm particle, Dionex) at a flow rate of 8 μl/min (35–37). Peptides not bound to the TiO_2 trap were trapped on a Acclaim® Pepmap 100 reversed phase trap (100 μm inner diameter $\times$ 2 cm, 5 μm particle, 100 Å pore, C18) (Dionex) (supplemental Fig. S1*A*), after which the reversed phase trap was switched in line with nano-flow pumps and the analytical column was packed in-house with Magic C18AQ stationary phase (Michrom Bioresources, Auburn, CA) (75 μm inner diameter $\times$ 15 cm, 5 μm particle, 200 Å pore) and subsequently analyzed via MS (supplemental Fig. S1*C*). Peptides were eluted from the analytical column with mobile phases A and B consisting of 0.1% formic acid in water and acetonitrile, respectively. The elution profile consisted of an initial solvent composition of 2% B for 5 min, followed by a gradient from 10% to 45% B over 120 min. The column was then cleaned with 90% B for 6 min before re-equilibrating at 2% B for 13 min at a 300 nl/min flow rate. After the elution and MS analysis of unbound peptides, a separate method was utilized to wash nonspecific bound peptides to waste using a 40-μl bolus of 80% acetonitrile, 20% water, 0.1% HFBA, and 2 mg/ml dihydroxybenzoic acid (2 $\times$ 20 μl injections)(supplemental Fig. S1*B*). Remaining peptides bound to the TiO_2 trap were eluted to the reversed phase trap with a 40-μl bolus of 200 mM ammonium bicarbonate pH 9.4, followed by elution from the reversed phase trap and separation on the analytical column as described above for unbound peptides (supplemental Fig. S1*C*).

LTQ-FT MS—Mass spectrometric analysis was performed on a hybrid LTQ-FT Ultra (ThermoFisher Scientific, San Jose, CA) equipped with a 7 Tesla superconducting magnet (38). The pulse sequence consisted of seven events, including a broadband acquisition in profile mode with a resolving power of 100,000 at $m/z = 400$. Broadband acquisition was followed by six data-dependent MS/MS events acquired in the linear ion trap. MS/MS was performed on the top six most abundant precursors from the broadband scan having a minimum signal of 800 with a 2 m/z isolation width and collision-induced dissociation fragmentation at a normalized collision energy of 35% for 30 ms. The automatic gain control limits for the linear ion trap and ion cyclotron resonance cell were 1×10^5 and 2×10^6, respectively. Charge state screening was used to exclude precursors having charges of 1^+ and greater than 4^+ from fragmentation. Additionally, a 45-s dynamic exclusion was implemented after one repeat count within 30 s of first detection of a precursor mass with an exclusion window of $\pm$20 ppm to reduce redundant analyses of abundant precursor ions that might dominate the mass spectra for long periods of time.

Protein Identification and Quantification—Data files in .RAW format were submitted for protein identification and SILAC quantification in MaxQuant (version 1.1.1.25) (39) using the integrated search algorithm Andromeda (40) to search the UniProt Human database (downloaded February 10, 2010, from the European Bioinformatics Institute and consisting of 26,404 entries), in addition to a database of common contaminants. Searches were performed with a $\pm$7 ppm precursor mass tolerance and a 0.6-Da fragment mass tolerance. Peptides of at least six amino acids and with a maximum of two missed cleavages were allowed for the analysis. Variable modifications allowed in the search included methionine oxidation and phosphorylation of serine, threonine, and tyrosine. A fixed modification for the carbamidomethylation of cysteine was also used. Andromeda reported results with a 1% peptide and protein false discovery rate (FDR). Proteins were identified only if they had two or more peptides meeting the FDR cutoff. Phosphorylation sites were identified with a 5% FDR with subsequent manual validation of their MS/MS spectra for precursor and fragment mass accuracies and percent coverage of the total spectrum intensity by the assigned sequence. Signals from peptides matching to multiple proteins were attributed proportionally based on the signal intensity of their unique peptides. Protein isoforms were identified by their unique peptides. Quantification was performed on all unique and razor peptides for a given protein, allowing for unmodified, oxidized, and phosphorylated peptides. The resulting protein quantitation values were also manually verified. MaxQuant output files containing quantitative protein data were further analyzed in Perseus, in which the Significance B calculation was used to determine statistically significant changes in protein ratios, taking into account the variation of protein ratios in addition to their abundance (39).

Annotation and Gene Ontology—Uniprot accession numbers for proteins identified within MaxQuant were mapped to their corresponding Ensembl gene identifications and uploaded to the gene ontology program PANTHER (Protein Analysis through Evolutionary Relationships, version 7.0) (41, 42). Gene lists were classified using the PANTHER classification terms, and the list of total genes, genes with significantly increased protein ratios, and genes with significantly decreased protein ratios were compared with the NCBI Homo sapiens genome in order to determine which biological processes and pathways were statistically significant and overrepresented in our lists. p values were determined via binomial statistic.

Western Blot for Protein Ratio Validation—Primary antibodies for CDCP1, focal adhesion kinase (FAK), Paxillin, HER4, and EGFR were obtained from Cell Signaling Technologies. Anti-phosphotyrosine (4G10) antibody was obtained from Millipore. Immunopurification for Western blot analyses was carried out with the incubation of 1 to 2 μg of primary antibody with 1 mg of protein overnight at 4 °C. Antibody–antigen complexes were captured with protein A/G beads (Pierce) and run on SDS-PAGE.

siRNA Screen—Functional studies were performed using a Dharmacon (Lafayette, CO) custom siRNA library. Two separate siRNA libraries were generated after gene accessions were submitted to Dharmacon for identified proteins with increased protein ratios in the $SkBr3^R$ cells and the $BT474^R$ cells. Pooled siRNAs with four siRNAs per target were received in a 96-well format, reconstituted in nuclease-free water, and aliquotted into daughter 96-well plates for a stock concentration of 2 μM.

Lipofectamine™ RNAiMAX (Invitrogen) reagent was incubated with the siRNA, allowed to complex for 20 min, and distributed over six 96-well plates. Trastuzumab-resistant cells were seeded at 6400 cells per well and incubated at 37 °C overnight to achieve optimal transfection efficiency. The final concentration of siRNA was 25 nM. ERBB2 siRNA (Ambion) was used as a positive control. siGENOME nontargeting siRNA pool #2 (Dharmacon), a control siRNA-A with a scrambled sequence (Santa Cruz), and a mock-treated sample that received transfection reagent only served as negative controls. Media was changed 24 h post-transfection; three replicate plates received media, and three replicate plates received media plus 100 μg/ml trastuzumab. Cells were cultured for 7 days, and media with or without trastuzumab was refreshed two times during that period. After 7 days, all six plates were treated with Alamar Blue (Invitrogen) and incubated for 2 h, and fluorescence measurements were made using a multi-mode plate reader (BioTek Synergy H4 plate reader, Winooski, VT) at an excitation wavelength of 540 nm and an emission wavelength of 585 nm, as per Ref. 43. Background fluorescence was subtracted from the raw fluorescence values and normalized to untransfected cells. Averages were taken across the three replicate plates of two independent replicate experiments for each condition. The fold change was defined as the relative fluorescence unit value for cells treated with siRNA plus 100 μg/ml trastuzumab as compared to that of cells treated with siRNA only.

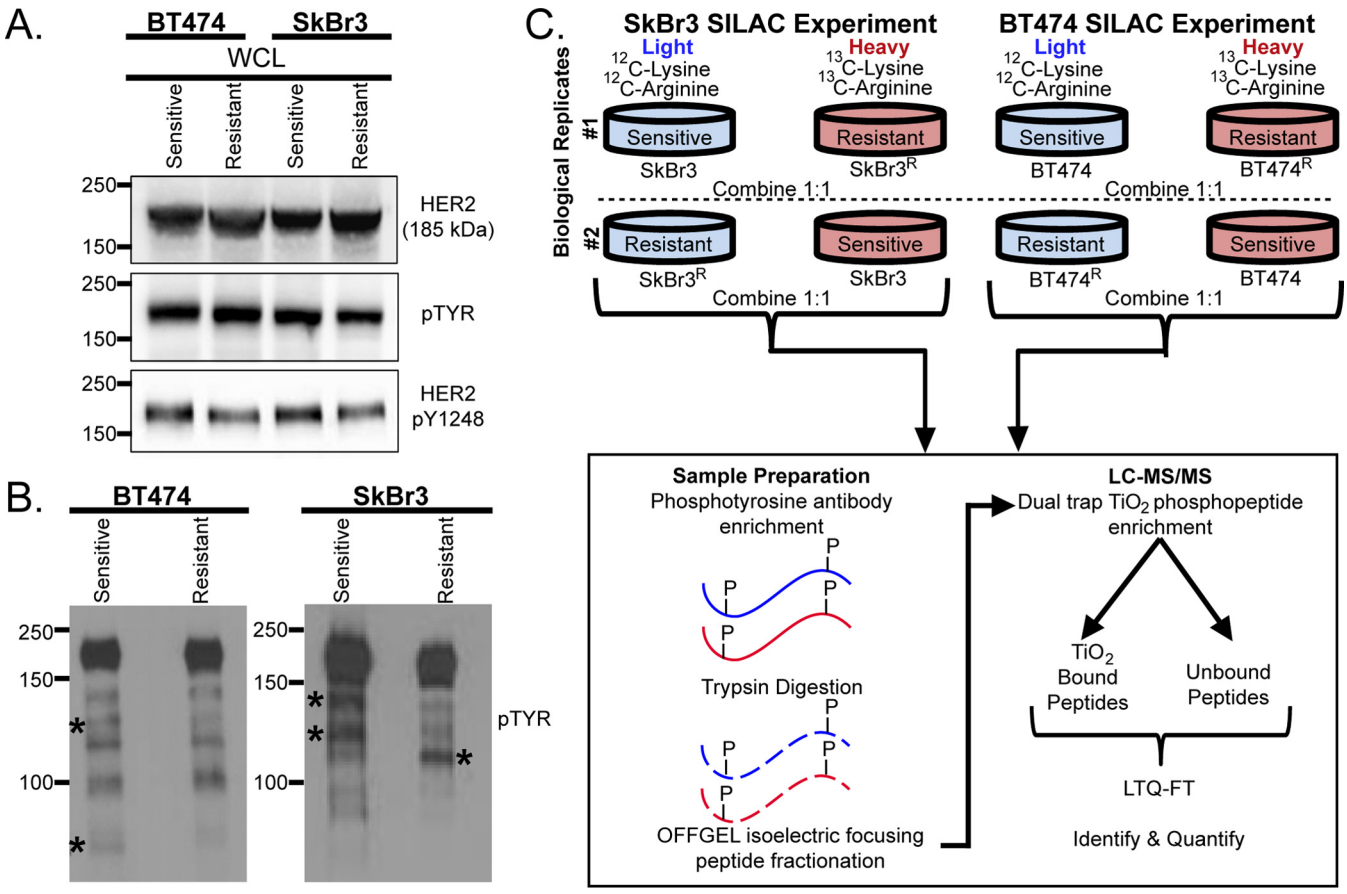

FIG. 1. **Altered tyrosine phosphorylation patterns between trastuzumab-sensitive and trastuzumab-resistant cell lines.** *A*, immunoblot of HER2 protein expression and phosphorylation in whole cell lysates (WCL) from SkBr3/SkBr3^R and BT474/BT474^R pairs of cell lines. SkBr3^R and BT474^R denote the respective trastuzumab-resistant cell lines. *B*, lysates from SkBr3, SkBr3^R, BT474, and BT474^R cells were subjected to phosphotyrosine immunoprecipitation (using 4G10 antibody) and then immunoblotted with the same phosphotyrosine antibody. Asterisks represent differences in phosphoprotein bands seen between the respective trastuzumab-sensitive and -resistant cell lines. *C*, experimental workflow for SILAC labeling and LC-MS/MS.

RESULTS

Quantitative Proteomic Strategy—Trastuzumab-resistant cells, established in the laboratory of Dr. Dennis Slamon, were derived from the parental lines after 9 months of selection in 100 μg/ml trastuzumab (32). HER2 expression and phosphorylation levels were essentially the same in the sensitive and resistant cell lines (Fig. 1*A*). The resistant cell lines retained a dependence on HER2 signaling and were growth-inhibited by the HER2 tyrosine kinase inhibitor lapatinib (32) and by HER2 siRNA (supplemental Fig. S2). However, multiple differences in the overall tyrosine phosphorylation pattern were seen between the sensitive and resistant cell line pairs (Fig. 1*B*). In order to identify and quantify these phosphotyrosine-containing proteins, we used SILAC as a strategy to differentially label the trastuzumab sensitive and resistant pairs of cells (24, 44). Fig. 1*C* shows a two-state SILAC strategy in which the sensitive cells were labeled with $^{12}C_6$-L-arginine and $^{12}C_6$-L-lysine (light) and the resistant cells were labeled with $^{13}C_6$-L-arginine and $^{13}C_6$-L-lysine (heavy). A second biological replicate experiment was performed with the labeling reversed. Phosphotyrosine-containing proteins were enriched via immunoprecipitation with 4G10 and PY100 antibodies. After immunoprecipitation, the proteins were eluted with phenyl phosphate, acetone precipitated, and digested with trypsin. The resulting tryptic peptides were separated into 12 fractions using isoelectric focusing (IEF). The IEF fractions were loaded on the LC-MS system, and a second phospho-enrichment was performed using a dual-trapping method employing titanium dioxide (TiO_2) and reversed phase packing materials (45). Both TiO_2 bound and unbound fractions were analyzed using an LTQ-FT for protein identification. The MaxQuant computational platform running the Andromeda search algorithm was used to identify proteins at a 1% FDR (40). The average percent error of quantification was ~22% across both datasets. The average percent sequence coverage was 11.7% for the SkBr3 dataset and 9.6% for the BT474 dataset (supplemental Table S1).

The resulting SILAC protein ratios were calculated from the respective extracted ion chromatograms of phosphopeptides and non-modified peptides mapping to these proteins. The

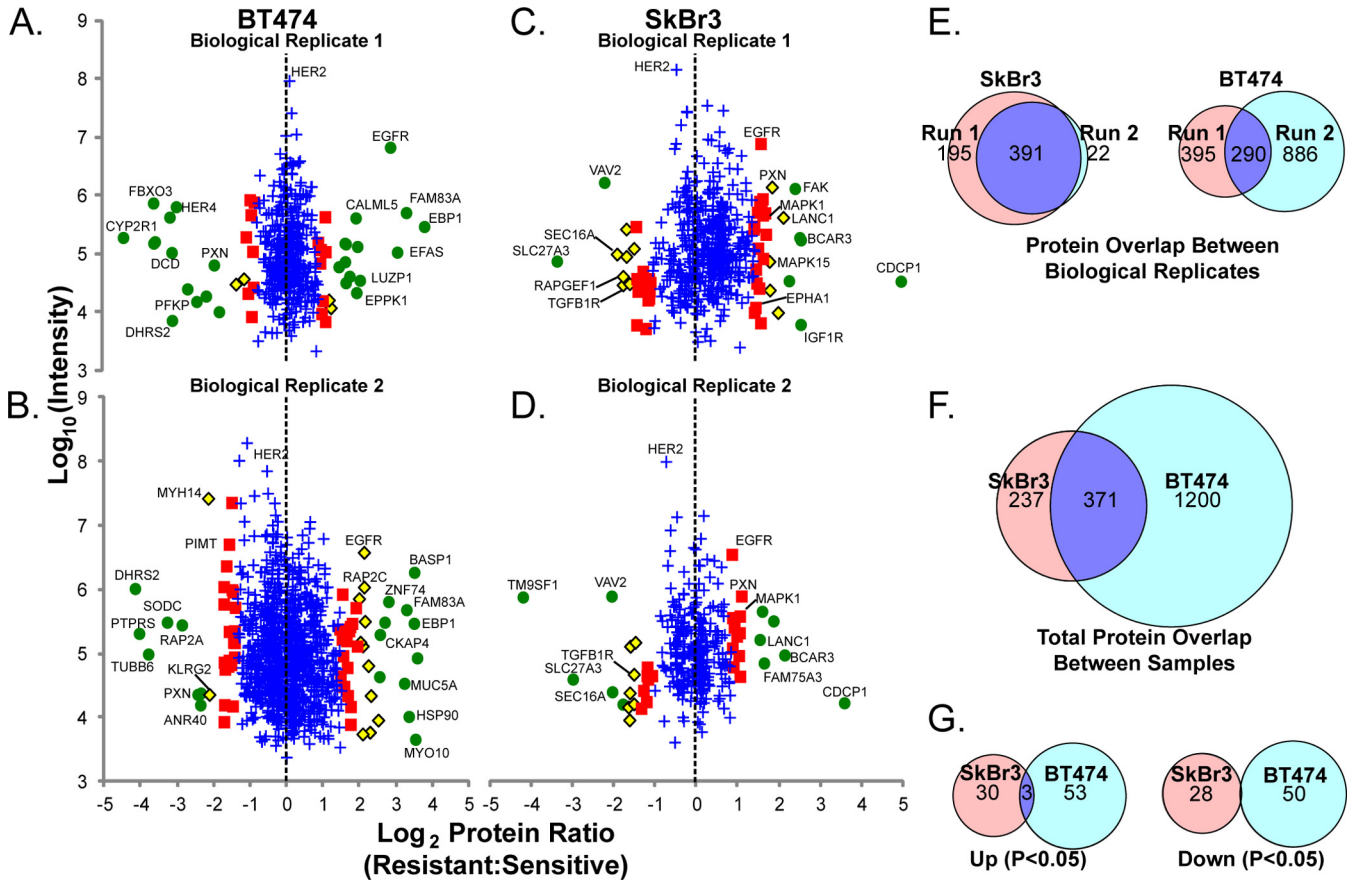

FIG. 2. **Distribution of protein ratios from identified proteins in the SkBr3/SkBr3^R and BT474/BT474^R SILAC experiments.** *A–D*, volcano plots showing the protein ratios (in $\log_2$) as a function of the log intensity for each inferred protein. Green circles are proteins with a p value of <0.001 as determined by the Perseus Significance B calculation, yellow diamonds are proteins with a p value between 0.001 and 0.01, red squares represent p values between 0.01 and 0.05, and blue crosses are proteins whose fold change is not significant ($p > 0.05$). Protein ratios are resistant:sensitive (heavy:light), and the log intensity of the proteins is the sum of peptide ion intensities for that protein. *E*, comparison of biological replicates (rep.) 1 and 2 in the SkBr3/SkBr3^R and BT474/BT474^R datasets. *F*, comparison of all proteins identified from each dataset. *G*, comparison of proteins with significantly increasing/decreasing ratios in both datasets.

protein ratios represent the relative abundance of phosphotyrosine-containing proteins and their interactors in the trastuzumab-resistant cell line compared with its parental, trastuzumab-sensitive cell line. The distribution of protein ratios (Fig. 2*A–2D*) demonstrated that a majority of identified proteins were unchanged and clustered at a 1:1 protein ratio (0 on the $\log_2$ scale). This is expected with the analysis of paired parental and daughter cell lines. A smaller fraction of proteins showed significant quantitative change ($p < 0.05$ according to Significance B calculation in Perseus). In these experiments, protein ratios that show significant change are suggestive of changes in protein phosphorylation, though other processes such as protein–protein interactions and large changes in protein expression could also affect the protein ratio. It is reasonable to hypothesize that proteins that exhibit significant change in protein ratios might contribute to the resistant phenotype and, with further biological validation, might be potential drug targets for overcoming or reversing trastuzumab resistance.

Proteomic Identifications—In the SkBr3 cell pair, 33 proteins showed a significantly increased protein ratio, and 28 proteins showed a significantly decreased protein ratio (Table I, Table III, and supplemental Table S1). In the BT474 cell pair, 56 proteins showed a significantly increased protein ratio, and 50 proteins showed a significantly decreased protein ratio (Table II, Table III, and supplemental Table S1). In order to obtain a global view of which biological processes and pathways were overrepresented in both SILAC datasets, we used PANTHER (41). The PANTHER analysis of biological pathways indicated that our phosphotyrosine enrichment strategy successfully resulted in the overrepresentation of several signaling pathways in SkBr3 (supplemental Fig. S3) and BT474 (supplemental Fig. S4). These signaling pathways include the EGFR, IGF1R, and PDGFR tyrosine kinase signaling pathways. Full results of the PANTHER analysis are provided in supplemental Table S2.

SkBr3 Dataset—CUB domain containing protein 1 (CDCP1)/Trask was identified as the protein with the greatest

TABLE I
Proteins with significantly increased resistant:sensitive protein ratios in SkBr3

Uniprot ID	Protein name	Protein description	Ratio ($SkBr3^R$:SkBr3)	*P* value
Q9H5V8	CDCP1	CUB domain-containing protein 1	12.1	6.89×10^{-16}
O75815	BCAR3	Breast cancer anti-estrogen resistance protein 3	4.4	1.39×10^{-6}
B4DYR9	B4DYR9	cDNA FLJ56363	3.7	2.49×10^{-5}
P08069	IGF1R	Insulin-like growth factor 1 receptor	3.6	6.17×10^{-5}
B4E2N6	PTK2	Focal adhesion kinase 1, PTK2	3.4	1.73×10^{-4}
A1L0S7	A1L0S7	TNS1 protein (fragment)	3.1	2.08×10^{-4}
Q658W2	Q658W2	Putative uncharacterized protein DKFZp666O0110	3.0	3.16×10^{-4}
Q08380	LGALS3BP	Galectin-3-binding protein	3.1	4.67×10^{-4}
O43813	LANC1	LanC-like protein 1	2.9	5.23×10^{-4}
Q7Z4W1	DCXR	L-xylulose reductase	2.7	2.88×10^{-3}
P49023	PXN	Paxillin	2.5	6.58×10^{-3}
O14966	RAB7L1	Ras-related protein Rab-7L1	2.4	8.70×10^{-3}
Q8TD08	MAPK15	Mitogen-activated protein kinase 15	2.4	9.20×10^{-3}
P28482	MAPK1	Mitogen-activated protein kinase 1	2.3	1.40×10^{-2}
Q59FC3	Q59FC3	G protein-coupled receptor kinase interactor 1 variant	2.1	1.56×10^{-2}
B4DEV4	BCAR1	Breast cancer anti-estrogen resistance protein 1	2.2	1.80×10^{-2}
Q9H223	EHD4	EH domain-containing protein 4	2.1	1.91×10^{-2}
B7Z6G2	ARHGEF7	Rho guanine nucleotide exchange factor 7	2.2	2.20×10^{-2}
Q13907	IDI1	Isopentenyl-diphosphate delta-isomerase 1	2.1	2.40×10^{-2}
Q06830	PRDX1	Peroxiredoxin-1	2.0	2.46×10^{-2}
O14732	IMPA2	Inositol monophosphatase 2	2.1	2.84×10^{-2}
B4E1G6	GALK1	Galactokinase 1	2.1	3.19×10^{-2}
P62937	PPIA	Peptidyl-prolyl cis-trans isomerase A	2.0	3.42×10^{-2}
Q93052	LPP	Lipoma-preferred partner	2.0	3.72×10^{-2}
P13489	RNH1	Ribonuclease inhibitor	2.0	4.00×10^{-2}
B7ZLR1	B7ZLR1	VAV3 protein	1.9	4.02×10^{-2}
P21709	EPHA1	Ephrin type-A receptor 1	2.0	4.17×10^{-2}
P48735	IDHP	Isocitrate dehydrogenase [NADP], mitochondrial	1.8	4.55×10^{-2}
P55084	ECHB	Trifunctional enzyme subunit beta, mitochondrial	1.8	4.67×10^{-2}
P10909	CLU	Clusterin	2.0	4.74×10^{-2}
P00533	EGFR	Epidermal growth factor receptor	1.8	4.92×10^{-2}
P15311	EZR	Ezrin	2.0	4.99×10^{-2}

protein ratio in our SkBr3 SILAC sample (Table I; protein ratio 12.1). CDCP1/Trask is a transmembrane protein that can be phosphorylated by the Src family of tyrosine kinases (47). CDCP1/Trask is a downstream target of the hypoxia inducible factor HIF1 and plays a critical role in kidney cancer cell migration (48). CDCP1/Trask was identified in a prior SILAC study comparing highly metastatic to low metastatic melanoma cells and was found to be associated with the highly metastatic phenotype (47). Functional studies show that CDCP1/Trask is regulated by the Src family kinases, specifically Fyn, and regulates cell–cell and cell–matrix adhesion through Protein Kinase C δ (47–49).

FAK (PTK2/FAK) and Paxillin (PXN) also showed significantly increased protein ratios. FAK and PXN localize to focal adhesions, play a key role in integrin signaling, and affect cell migration and cell adhesion (50, 51). FAK is a cytoplasmic tyrosine kinase, and it can form a complex with Src family kinases (50). Dephosphorylation or down-regulation of FAK and PXN by EGFR and HER2 signaling has been previously reported in two phosphoproteomic studies (24, 52). Activation of FAK occurs in pancreatic and other cancers, and FAK inhibitors are undergoing drug development (53, 54).

Several receptor tyrosine kinases showed significantly increased protein ratios. Insulin-like growth factor-1 receptor (IGF1R) and EGFR are known proteins involved in mechanisms of trastuzumab resistance and showed protein ratios of 3.6 and 1.8, respectively. The activation of IGF1R or EGFR leads to persistent signaling to downstream proteins, bypassing the inhibitory effects of trastuzumab on HER2-positive breast cancer cells (5, 6). Similarly, the Ephrin receptor EPHA1 showed a protein ratio of 2.0. Ephrin receptors play a role in the induction of angiogenesis, and they are also involved in the promotion of cell motility, attachment, and migration through activation of the PI3K/AKT signaling pathway (55).

Notable proteins that showed a significant decrease in protein ratio included transforming growth factor β receptor I (TGFBR1)/ALK5 (Table III; protein ratio = 0.4). TGFBR1/ALK5 is a cell surface receptor and serine/threonine kinase that can act both as a tumor suppressor and as a pro-oncogenic factor. It is reported to be directly involved in breast cancer and pancreatic adenocarcinomas (56–59). Other proteins that showed a decreased protein ratio are the guanine nucleotide exchange factors VAV2 and RAPGEF1.

TABLE II
Proteins with significantly increased resistant:sensitive protein ratios in BT474

Uniprot ID	Protein name	Protein description	Ratio ($BT474^R$:BT474)	*P* value
Q9UQ80	EBP1/PA2G4	ErbB-3 binding protein 1/proliferation-associated protein 2G4	13.6	1.71×10^{-20}
Q86UY5	FAM83A	Protein FAM83A	9.7	8.69×10^{-16}
O43281	EFS	Embryonal Fyn-associated substrate	8.2	1.02×10^{-13}
P00533	EGFR	Epidermal growth factor receptor	7.2	3.34×10^{-12}
Q86V48	LUZP1	Leucine zipper protein 1	4.1	9.71×10^{-7}
Q9HD67	MYO10	Myosin-X	11.8	1.05×10^{-6}
Q59EG8	Q59EG8	Proteasome 26S non-ATPase subunit 2 variant	12.2	1.83×10^{-6}
P11413	G6PD	Glucose-6-phosphate 1-dehydrogenase	3.9	2.38×10^{-6}
P80723	BASP1	Brain acid soluble protein 1	11.5	3.11×10^{-6}
P58107	EPPK1	Epiplakin	3.8	3.23×10^{-6}
Q5T9W8	Q5T9W8	Heat shock protein 90kDa alpha (cytosolic), class B member 1	10.4	3.86×10^{-6}
Q9NZT1	CALML5	Calmodulin-like protein 5	3.8	4.03×10^{-6}
P98088	MUC5A	Mucin-5AC (fragments)	9.5	8.85×10^{-6}
P37268	FDFT1	Squalene synthetase	3.3	2.82×10^{-5}
Q9BVG4	CXorf26	UPF0368 protein Cxorf26	3.1	8.47×10^{-5}
A8MXZ4	GPRC5C	Putative uncharacterized protein GPRC5C	3.1	1.05×10^{-4}
P10909	CLU	Clusterin	3.1	1.10×10^{-4}
A8K5P3	A8K5P3	Zinc finger protein 74 (Cos52)	7.0	1.88×10^{-4}
A7Y9J9	A7Y9J9	Mucin 5AC, oligomeric mucus/gel-forming	6.6	3.19×10^{-4}
P21291	CSRP1	Cysteine and glycine-rich protein 1	5.9	5.00×10^{-4}
P45954	ACADSB	Short/branched chain specific acyl-CoA dehydrogenase, mitochondrial	2.7	5.50×10^{-4}
Q07065	CKAP4	Cytoskeleton-associated protein 4	6.0	5.99×10^{-4}
Q59G88	Q59G88	Putative uncharacterized protein	5.7	6.68×10^{-4}
P01034	CYTC	Cystatin-C	5.0	1.81×10^{-3}
Q9ULT8	HECD1	E3 ubiquitin-protein ligase HECTD1	4.9	2.06×10^{-3}
Q99536	VAT1	Synaptic vesicle membrane protein VAT-1 homolog	4.7	2.54×10^{-3}
O15551	CLD3	Claudin-3	4.4	4.25×10^{-3}
P22307	SCP2	Non-specific lipid-transfer protein	2.3	4.36×10^{-3}
Q9Y3L5	RAP2C	Ras-related protein Rap-2c	4.4	4.67×10^{-3}
Q8N1F7	NUP93	Nuclear pore complex protein Nup93	4.3	5.18×10^{-3}
P15941	MUC1	Mucin-1	4.3	5.48×10^{-3}
P09543	CNP	2′,3′-cyclic-nucleotide 3′-phosphodiesterase	2.2	6.52×10^{-3}
O75487	GPC4	Glypican-4	4.1	7.11×10^{-3}
Q9BTI6	Q9BTI6	FLOT2 protein	4.0	8.17×10^{-3}
P24593	IBP5	Insulin-like growth factor-binding protein 5	3.9	9.09×10^{-3}
B4E2S3	B4E2S3	cDNA FLJ56561	3.8	1.05×10^{-2}
Q8N357	C2orf18	Transmembrane protein C2orf18	2.1	1.12×10^{-2}
O95831	AIFM1	Apoptosis-inducing factor 1, mitochondrial	2.1	1.18×10^{-2}
P67936	TPM4	Tropomyosin alpha-4 chain	2.0	1.81×10^{-2}
B4DMN1	B4DMN1	Ras-related protein Rab-11A	3.4	1.82×10^{-2}
P31150	GDIA	Rab GDP dissociation inhibitor alpha	3.4	1.84×10^{-2}
B1ANH3	B1ANH3	Guanylate kinase 1	3.4	2.02×10^{-2}
Q9Y4L1	HYOU1	Hypoxia up-regulated protein 1	2.0	2.22×10^{-2}
Q14764	MVP	Major vault protein	3.3	2.40×10^{-2}
B9ZVM9	B9ZVM9	Putative uncharacterized protein TCP10L2	3.3	2.55×10^{-2}
P00558	PGK1	Phosphoglycerate kinase 1	1.9	2.60×10^{-2}
P55084	HADHB	Trifunctional enzyme subunit beta, mitochondrial	1.9	2.95×10^{-2}
Q14395	Q14395	Mucin (fragment)	3.1	3.45×10^{-2}
Q6W4X9	MUC6	Mucin-6	3.0	3.49×10^{-2}
A0MZ66	SHOT1	Shootin-1	3.0	3.53×10^{-2}
Q4JM47	Q4JM47	AGR2	3.0	3.82×10^{-2}
O14745	SLC9A3R1	Na(+)/H(+) exchange regulatory cofactor NHE-RF1	1.8	4.13×10^{-2}
Q8WXQ7	Q8WXQ7	Propionyl coenzyme A carboxylase, alpha polypeptide	2.8	4.70×10^{-2}
B7Z2Z4	B7Z2Z4	Propionyl-CoA carboxylase beta chain, mitochondrial	2.9	4.83×10^{-2}
O75223	GGCT	Gamma-glutamylcyclotransferase	2.9	4.92×10^{-2}

BT474 Dataset—ErbB3 binding protein 1 (EBP1)/proliferation-associated protein 2G4 (PA2G4) (protein ratio = 13.6) and FAM83A (protein ratio = 9.7) were identified as the proteins with the greatest protein ratios in our BT474 SILAC sample (Table II). EBP1/PA2G4 is a negative regulator of HER3/ERBB3. EBP1/PA2G4 interacts with the juxtamem-

TABLE III
Select proteins with significantly decreased resistant:sensitive protein ratios in SkBr3 and BT474

Uniprot ID	Protein name	Protein description	Ratio	*P* value
		SkBr3 SILAC experiment	**(SkBr3^{R}:SkBr3)**	
B7Z6C9	B7Z6C9	Transmembrane 9 superfamily protein member 1	0.1	5.31×10^{-16}
P04264	KRT1	Keratin, type II cytoskeletal 1	0.1	2.21×10^{-9}
Q5K4L6	SLC27A3	Long-chain fatty acid transport protein 3	0.1	1.86×10^{-7}
O15027	SC16A	Protein transport protein Sec16A	0.2	8.80×10^{-5}
P52735	VAV2	Guanine nucleotide exchange factor VAV2	0.3	3.34×10^{-4}
P50454	SERPH	Serpin H1	0.3	6.01×10^{-4}
Q8IV73	RAPGEF1	Rap guanine nucleotide exchange factor (GEF) 1	0.3	2.92×10^{-3}
Q8WVX9	FAR1	Fatty acyl-CoA reductase 1	0.4	4.19×10^{-3}
Q96BI1	SLC22A18	Solute carrier family 22 member 18	0.4	4.25×10^{-3}
P36897	TGFBR1	TGF-beta receptor type-1	0.4	5.98×10^{-3}
Q9P0V3	SH3BP4	SH3 domain-binding protein 4	0.4	9.28×10^{-3}
Q9NYV4	CRKRS	Cell division cycle 2-related protein kinase 7	0.4	1.32×10^{-2}
P52701	MSH6	DNA mismatch repair protein Msh6	0.4	1.33×10^{-2}
A6NJ78	METT5D1	S-adenosyl-L-methionine-dependent methyltransferase METT5D1	0.4	1.49×10^{-2}
P15924	DESP	Desmoplakin	0.4	2.08×10^{-2}
Q63HN8	RN213	RING finger protein 213	0.4	2.20×10^{-2}
Q8IUX1	T126B	Transmembrane protein 126B	0.4	2.52×10^{-2}
Q9NVI7	ATAD3A	ATPase family AAA domain-containing protein 3A	0.5	3.03×10^{-2}
Q9C0E2	XPO4	Exportin-4	0.5	3.65×10^{-2}
P05026	ATP1B1	Sodium/potassium-transporting ATPase subunit beta-1	0.5	3.96×10^{-2}
P06703	S100A6	Protein S100-A6	0.5	4.00×10^{-2}
Q9UBF2	COPG2	Coatomer subunit gamma-2	0.5	4.04×10^{-2}
Q14527	HLTF	Helicase-like transcription factor	0.5	4.19×10^{-2}
Q9HC07	TMEM165	Transmembrane protein 165	0.5	4.45×10^{-2}
		BT474 SILAC experiment	**(BT474^{R}:BT474)**	
Q6VVX0	CYP2R1	Vitamin D 25-hydroxylase	0.0	5.03×10^{-23}
Q9UK99	FBXO3	F-box only protein 3	0.1	6.74×10^{-16}
Q9Y6S9	RPS6KL1	Ribosomal protein S6 kinase-like 1	0.1	7.60×10^{-16}
Q8N3P4	VPS8	Vacuolar protein sorting-associated protein 8 homolog	0.1	1.47×10^{-15}
Q59H77	CCT3	Chaperonin containing TCP1, subunit 3 (gamma) variant (fragment)	0.1	1.27×10^{-12}
P81605	DCD	Dermcidin	0.1	3.08×10^{-12}
Q13268	DHRS2	Dehydrogenase/reductase SDR family member 2	0.1	3.69×10^{-12}
Q15303	ERBB4	Receptor tyrosine-protein kinase erbB-4	0.1	1.93×10^{-11}
P02452	COL1A1	Collagen alpha-1(I) chain	0.2	1.61×10^{-9}
Q13332	PTPRS	Receptor-type tyrosine-protein phosphatase S	0.1	2.52×10^{-9}
Q2NKY5	Q2NKY5	TUBB6 protein	0.1	2.40×10^{-8}
Q01813	PFKP	6-phosphofructokinase type C	0.2	4.06×10^{-8}
Q08554	DSC1	Desmocollin-1	0.2	8.77×10^{-7}
P00441	SODC	Superoxide dismutase [Cu-Zn]	0.1	1.53×10^{-6}
Q59GS5	PXN	Paxillin	0.3	9.06×10^{-6}
P10114	RAP2A	Ras-related protein Rap-2a	0.2	2.60×10^{-5}
Q9Y5V3	MAGED1	Melanoma-associated antigen D1	0.3	3.56×10^{-5}
P27105	STOM	Erythrocyte band 7 integral membrane protein	0.3	3.63×10^{-4}
Q6AI12	ANR40	Ankyrin repeat domain-containing protein 40	0.3	5.34×10^{-4}
B0I1S2	B0I1S2	MYH14 variant protein	0.3	1.59×10^{-3}
A4D1S0	KLRG2	Killer cell lectin-like receptor subfamily G member 2	0.3	1.66×10^{-3}
O95396	MOCS3	Adenylyltransferase and sulfurtransferase MOCS3	0.5	6.82×10^{-3}
Q13829	TNAP1	BTB/POZ domain-containing protein TNFAIP1	0.4	1.05×10^{-2}
O14974	MYPT1	Protein phosphatase 1 regulatory subunit 12A	0.4	1.29×10^{-2}
P56537	EIF6	Eukaryotic translation initiation factor 6	0.5	1.63×10^{-2}
P49915	GUAA	GMP synthase [glutamine-hydrolyzing]	0.5	1.70×10^{-2}
P16615	ATP2A2	Sarcoplasmic/endoplasmic reticulum calcium ATPase 2	0.5	2.20×10^{-2}
Q9GZZ1	NAT13	N-acetyltransferase 13	0.5	2.28×10^{-2}
P22061	PIMT	Protein-L-isoaspartate (D-aspartate) O-methyltransferase	0.5	2.34×10^{-2}
P55060	CSE1L	Exportin-2	0.5	2.57×10^{-2}
Q05639	EF1A2	Elongation factor 1-alpha 2	0.5	2.70×10^{-2}

TABLE III—*continued*

Uniprot ID	Protein name	Protein description	Ratio	*P* value
Q9HCY8	S100A14	Protein S100-A14	0.5	2.85×10^{-2}
Q9Y608	LRRF2	Leucine-rich repeat flightless-interacting protein 2	0.5	3.19×10^{-2}
Q92616	GCN1L1	Translational activator GCN1	0.5	3.35×10^{-2}
Q96IZ0	PAWR	PRKC apoptosis WT1 regulator protein	0.5	3.49×10^{-2}
B9EGR7	ARHGEF5	Rho guanine nucleotide exchange factor (GEF) 5	0.5	3.71×10^{-2}
P33993	MCM7	DNA replication licensing factor MCM7	0.5	4.06×10^{-2}
P62993	GRB2	Growth factor receptor-bound protein 2	0.5	4.10×10^{-2}
B4E3B6	HSPA1A	Heat shock 70 kDa protein 1	0.6	4.15×10^{-2}
P02786	TFR1	Transferrin receptor protein 1	0.5	4.37×10^{-2}

brane region of HER3 and Protein Kinase C (when HER3 is not ligand bound). Upon ligand binding, EBP1/PA2G4 dissociates from HER3 and translocates to the nucleus, where it associates with Rb and E2F regulated genes (60, 61). FAM83A (also called BJ-TSA-9 or TSGP) mRNA is expressed in 52% of lung cancer tissues and was shown to be a tumor marker in circulating lung cancer cells. Although the function of FAM83A remains unclear, a correlation with lung cancer disease progression has been identified (62, 63). Similar to SkBr3, EGFR also showed an increased protein ratio in the BT474 cell line pair with a protein ratio of 7.2. This supports the previous findings of EGFR involvement in trastuzumab resistance (5). Other proteins that showed an increased protein ratio are embryonal Fyn-associated substrate (EFS) (protein ratio = 8.2) and mitochondrial apoptosis-inducing factor 1 (AIFM1) (protein ratio = 2.1).

Notable proteins that showed a decrease in protein ratio (Table III) included MAGED1 (ratio = 0.24) and HER4/ERBB4 (ratio = 0.11). Melanoma antigen family D1 (MAGED1) exhibits anti-proliferative, anti-invasive, and anti-migratory effects in MCF-7 and MDA-MB-231 breast cancer cell lines and causes morphological changes and inhibition of neurite outgrowths in neuronal cells (64, 65). Recent genomic sequencing found MAGED1 to be mutated in 5% of multiple myeloma patients (66). HER4/ERBB4 is a member of the EGFR family of receptor tyrosine kinases and is known to have both tumor suppressive and pro-oncogenic activity (67). Some of the tumor-suppressive functions of HER4/ERBB4 include growth inhibition and induced differentiation (68). Elevated levels of HER4/ERBB4 expression are associated with favorable outcomes in breast cancer and decreased recurrence rates of ductal carcinoma *in situ*, the precursor lesion to breast cancer (67, 69, 70).

Signaling Networks are Context Dependent—We compared the two SILAC datasets on SkBr3 and BT474 cells to determine the degree of shared proteins. We hoped this would identify common proteins that might be involved in trastuzumab resistance. Signaling networks are context dependent, and although both SkBr3 and BT474 cells are HER2 gene amplified breast cancer cell lines, they have important differences. The SkBr3 cell line does not express estrogen receptor (ER) or progesterone receptor (PR) and was originally isolated from a metastatic site (malignant pleural fluid drained from a patient), whereas the BT474 cell line does express ER and PR and was isolated from a primary tumor in a patient's breast (46). Biological replicates 1 and 2 in the SkBr3 dataset showed a very high degree of overlap (Fig. 2*E*). The biological replicates for BT474 also showed a high degree of overlap, though it was not as high as in SkBr3 because BT474 replicate 2 yielded a higher total number of protein identifications. We then compared the proteins identified from the SkBr3 cell line to those from the BT474 cell line (Fig. 2*F*). We found 371 shared proteins between the two cell lines. 237 proteins were unique to the SkBr3 cells, and 1200 proteins were unique to the BT474 cells. Among the shared proteins, we found EGFR, HER2, HER3, SHC1, GRB2, GRB7, GAB1, ras-related protein RAN, regulatory subunits of PI3K, CTNND1, and CTNND2 (Fig. 2*F*). We further compared the number of proteins that demonstrated a significant increase or decrease in protein ratio between the two cell lines (Fig. 2*G*). We found only three shared proteins (EGFR, Clusterin-CLU, and HADHB) among the proteins with significant increases, and no shared proteins among the proteins with a significant decrease in ratio. We also noticed that there were proteins that had opposite protein ratio changes in the two cell lines. For example, PXN had a protein ratio of 2.5 in the SkBr3 cell pair (Table I) and a protein ratio of 0.3 in the BT474 cell pair (Table II). Similarly, the protein ratios for AIFM1 were 0.65 in SkBr3 and 2.1 in BT474. The number of shared proteins with a significantly increased or decreased protein ratio (Fig. 2*G*) is much smaller than the number of shared proteins between the cell lines or between the biological replicates (Figs. 2*F* and 2*E*), and these results suggest that there is a large degree of heterogeneity in the phosphotyrosine signaling network changes occurring in different trastuzumab-resistant cell lines.

Validation of Protein Ratios by Western Blots—Selected proteins from the BT474 and SkBr3 datasets were validated through immunoprecipitations and Western blots (Fig. 3). Changes in the protein ratio measured by SILAC can be due to changes in protein phosphorylation, protein expression, or a combination of both. Given that the goal of this paper is to identify and quantify protein changes in trastuzumab-resistant cells, any of these three possibilities is biologically important. EGFR gave a protein ratio of 7.2 in the BT474 dataset (Table

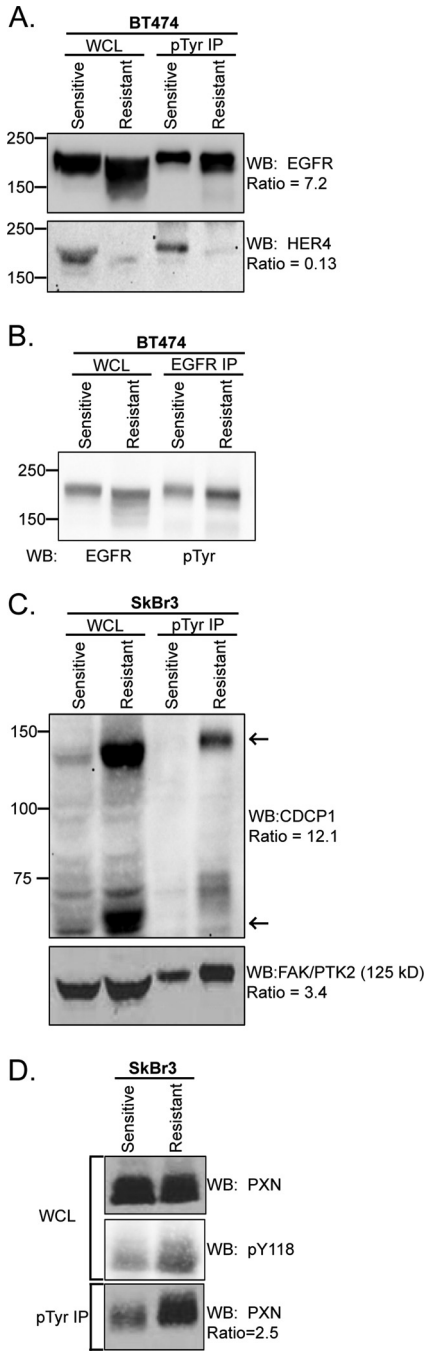

FIG. 3. **Validation of SILAC ratios with Western blots.** *A*, validation of EGFR and HER4 ratios in BT474 whole cell lysate (WCL) and phosphotyrosine (pTyr) IP. *B*, EGFR expression in BT474 WCL and EGFR phosphorylation by EGFR IP followed by Western blot (WB) for pTyr. *C*, validation of CDCP1 and FAK in SkBr3 WCL and pTyrIP. *D*, Western blot for Paxillin (PXN) and PXN pY 118 in WCL and pTyr IP in SkBr3 cells.

II). EGFR showed an increased expression level in the BT474^R cells relative to the trastuzumab-sensitive BT474 cells (Figs. 3*A* and 3*B*). The absolute amount of phosphorylated EGFR was measured by means of immunoprecipitation (IP) with anti-phosphotyrosine antibody and Western blot with EGFR antibody (Fig. 3*A*) or by the reverse IP-Western experiment (EGFR IP and Western blot with anti-phosphotyrosine antibody; Fig. 3*B*). Both results showed that the absolute level of phosphorylated EGFR was increased, matching the protein ratio measured by SILAC. HER4/ERBB4 was also measured via Western blot and showed a marked decrease in expression, matching its protein ratio measurement (Fig. 3*A*). In the SkBr3/SkBr3^R cell line pair, we measured CDCP1/Trask, FAK, and PXN (Figs. 3*C* and 3*D*). CDCP1/Trask is expressed as a 140-kDa glycoprotein and a 70-kDa cleavage product (48, 49). A marked increase in CDCP1/Trask expression was seen in SkBr3^R cells, and increased CDCP1/Trask protein was detected in the anti-phosphotyrosine IP from these cells. FAK showed comparable total expression levels but increased phosphorylation in the resistant cells, matching the measured protein ratio. PXN also showed similar total protein expression levels and increased phosphorylation in the resistant cells. The phospho-specific antibody to PXN pY118 and IP-Western blot showed similar changes in PXN phosphorylation, suggesting that the phosphotyrosine IP of cell lysates prior to proteomic analysis preserves the relative abundance of phosphorylation events in the native samples (Fig. 3*D*). A list of the 25 quantified phosphotyrosine sites from this study and their supporting MS/MS spectra are available in supplemental Table S3 and supplemental Figs. S5 and S6.

Functional Analysis of Identified Proteins—To determine whether the proteins identified via MS were functionally contributing to trastuzumab resistance, we performed a focused siRNA screen. A customized, small siRNA library to the proteins that had an increased ratio was purchased. The goal was to determine whether siRNA-mediated knockdown of these proteins could restore sensitivity to trastuzumab. The motivation for this siRNA screen was to rapidly determine which of the identified proteins had the largest functional role in trastuzumab resistance, thereby generating a prioritized list of proteins to pursue in later cell biology and clinical studies.

Positive and negative controls for this siRNA screen are shown in supplemental Fig. S2. siRNA to HER2 effectively reduced HER2 expression and cell viability and served as the positive control in this screen. Negative control siRNAs did not affect the viability of the trastuzumab-resistant cells, either on their own or in combination with trastuzumab. Figs. 4*A* and 4*B* show the fold change in cell viability for the siRNA plus trastuzumab treatment relative to the siRNA alone. Two independent siRNA experiments were performed on each cell line, and each experiment contained triplicate samples. siRNAs that restore trastuzumab sensitivity to the resistant cells will give fold changes < 1, which corresponds to negative values on the $\log_2$ fold change scale. siRNAs that do not affect trastuzumab resistance will give fold changes close to 1, corresponding to 0 on the $\log_2$ scale. The top hits from the siRNA screen are CDCP1/Trask, MAP kinase 1 (MAPK1), and PXN in the SkBr3^R cells and FAM83A, Epiplakin (EPPK1), and

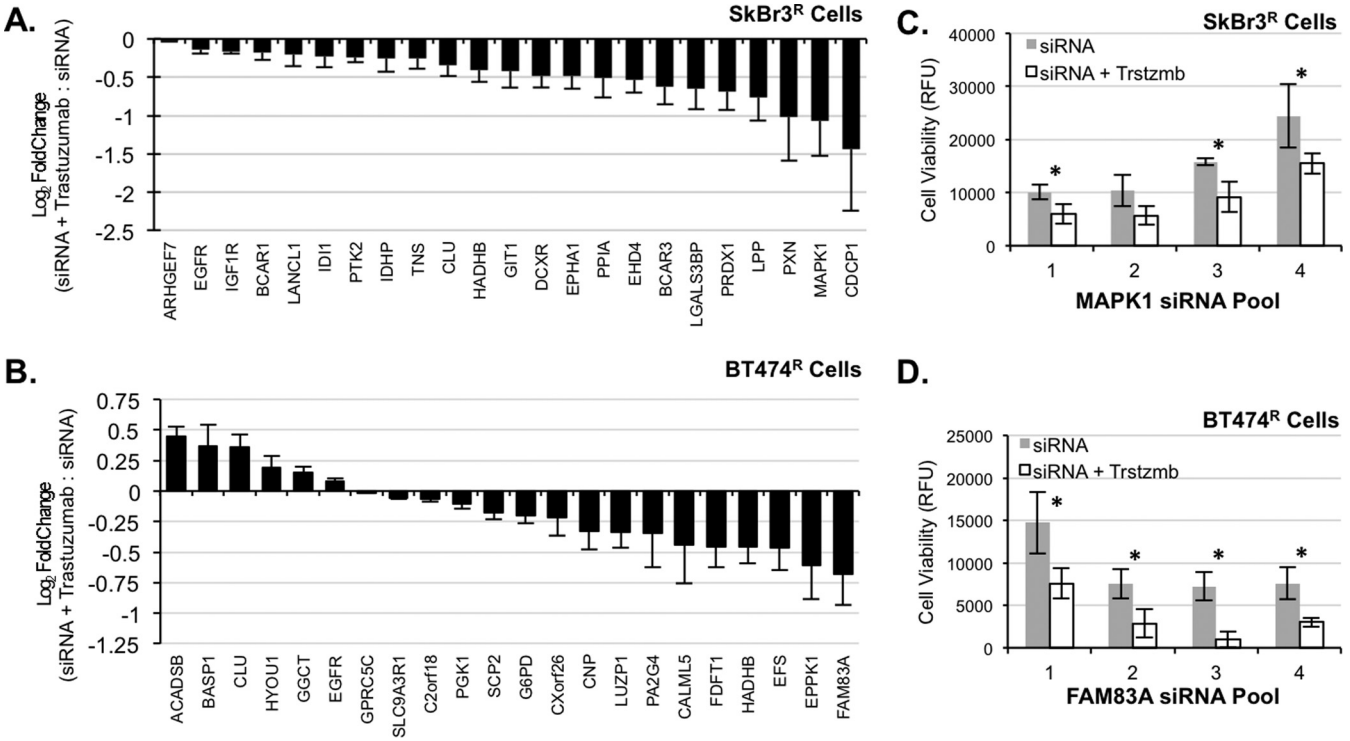

FIG. 4. **siRNA screen results.** *A*, selected siRNA results for SkBr3^R cells ($n = 3$) showing increasing magnitude of resensitization to trastuzumab from left to right. Error bars represent the 95% confidence limits. *B*, selected siRNA screen results for BT474^R cells ($n = 3$). Data in both *A* and *B* are representative of two independent experiments. *C*, responses of SkBr3R cells ($n = 3$) to individual siRNA targeting MAPK1. Asterisks denote significant difference in cell viability between siRNA only and siRNA + trastuzumab (Trstzmb). *D*, response of BT474 cells ($n = 3$) to individual siRNA targeting FAM83A. Full results for the siRNA screen are available in supplemental Table S4.

EFS in the BT474^R cells. This siRNA screen used a pool of four siRNAs to each protein target. In order to confirm the screen results, individual siRNAs to the top hits were tested. Figs. 4*C* and 4*D* show the effect of individual siRNAs to MAPK1 in SkBr3^R cells and FAM83A in BT474^R cells, respectively. For MAPK1 (Fig. 4*C*), three of the four individual siRNAs restored trastuzumab sensitivity, and for FAM83A (Fig. 4*D*), all four individual siRNAs restored trastuzumab sensitivity. The ability of multiple siRNAs to restore trastuzumab sensitivity increases our confidence in these protein targets. The top hits from this screen will receive the greatest attention in our future studies.

DISCUSSION

Trastuzumab resistance represents a serious medical problem, with most metastatic patients developing resistance over the course of their treatment, and this contributes to an increase in patient mortality. In this study, we used quantitative proteomics and phospho-enrichment methods to analyze the changes occurring in trastuzumab-resistant breast cancer cells. We identified both known and potentially novel trastuzumab resistance proteins. A comparison of results obtained from SkBr3 and BT474 cell pairs demonstrates that there is a high degree of diversity in trastuzumab resistance. The HER2 signaling network is known to be complex (22, 24), and multiple resistance mechanisms have been previously identified (12). These results demonstrate that individual breast cancers can develop trastuzumab resistance by a wide variety of means, suggesting that molecular tests to diagnose which resistance mechanisms are active in a patient could be highly clinically useful. The development of such molecular tests could potentially guide future treatment of trastuzumab-resistant HER2 gene amplified breast cancer patients.

A focused siRNA screen was performed to determine which proteins, of those that showed a significant quantitative change, were functionally relevant to the resistant phenotype. A focused siRNA screen of the proteomic identifications is a time- and cost-effective strategy to evaluate their functional role. The siRNA strategy was designed to identify which proteins might be good drug targets for overcoming trastuzumab resistance, and it employed a library tailored to the proteins with increased ratios in the resistant cells. A converse screening strategy using siRNA to induce resistance in the sensitive cells could yield functional information on proteins with a decreased ratio. This approach is conceptually similar to the genome-wide siRNA screen performed by Berns *et al.* (13).

Our quantitative phosphoproteomics-siRNA screening strategy revealed several proteins related to the Src kinase pathway, including CDCP1/Trask, embryonal Fyn-associated substrate, epiplakin, focal adhesion kinase, and Paxillin. Src

has recently emerged as a promising therapeutic target for overcoming trastuzumab resistance (11), and our finding that Src-interactors have a mitigating effect in resistant cells increases the confidence in these results. In addition, several novel proteins involved in trastuzumab resistance were identified. FAM83A is a putative prognostic marker for lung cancer, but its role in breast cancer is not known, and its ability to increase trastuzumab sensitivity in these studies warrants further investigation into its biological function. Knockdown of MAPK1 reversed trastuzumab resistance in SkBr3 cells, suggesting that combining MAP kinase pathway inhibitors with HER2 targeted drugs is a potential avenue for new therapy.

With the diversity of mechanisms that our study and others have indicated, there is an urgent need for diagnostic markers and therapeutic targets to guide the treatment of patients with trastuzumab-resistant breast cancers. The results from these analyses warrant future investigations into the specific roles that these novel proteins play in trastuzumab resistance.

Acknowledgments—We thank Michael L. Gross, Henry Rohrs, Leslie Hicks, and Sophie Alvarez for mass spectrometry instrument access and support. We also thank Dennis Slamon and Gottfried Konecny for generously providing the cell lines used in this study.

The data associated with this manuscript may be downloaded from the Proteome Commons Tranche using the following hash:

dCdKmk7RydWT76hBKX49gCu2yFHotyzqM9BsPDjGTXYQ5pch8PgvtS5EOYENrDZDafcZhUjf2z6BlliHcPGEBg+amtQAAAAAAABKhg==

The hash may be used to prove exactly what files were published as part of this manuscript's dataset, and the hash may also be used to check that the data have not changed since publication.

* This research was supported by grants from Susan G. Komen for the Cure, the 'Ohana Breast Cancer Research fund, and the Foundation for Barnes-Jewish Hospital. A.P.B. and T.S.C. are supported by NIH T32 training grants (Grant No. CA113275 for A.P.B. and Grant No. 2T32HL007088–36 for T.S.C.). Mass spectrometer instrument support was provided by the National Center for Research Resources of the NIH (Grant No. 2P41RR000954 to M. L. Gross).

S This article contains supplemental material.

** To whom correspondence should be addressed: Ron Bose, Tel.: 314-747-9308, Fax: 314-747-9320, E-mail: rbose@dom.wustl.edu.

§ These authors contributed equally to this work.

REFERENCES

1. Hynes, N. E., and Lane, H. A. (2005) ERBB receptors and cancer: the complexity of targeted inhibitors. *Nat. Rev. Cancer* **5,** 341–354
2. Slamon, D. J., Clark, G. M., Wong, S. G., Levin, W. J., Ullrich, A., and McGuire, W. L. (1987) Human breast cancer: correlation of relapse and survival with amplification of the HER-2/neu oncogene. *Science* **235,** 177–182
3. Slamon, D. J., Godolphin, W., Jones, L. A., Holt, J. A., Wong, S. G., Keith, D. E., Levin, W. J., Stuart, S. G., Udove, J., Ullrich, A., Press, M.F. (1989) Studies of the HER-2/neu proto-oncogene in human breast and ovarian cancer. *Science* **244,** 707–712
4. Burris, H. A., 3rd, Rugo, H. S., Vukelja, S. J., Vogel, C. L., Borson, R. A., Limentani, S., Tan-Chiu, E., Krop, I. E., Michaelson, R. A., Girish, S., Amler, L., Zheng, M., Chu, Y. W., Klencke, B., and O'Shaughnessy, J. A. (2011) Phase II study of the antibody drug conjugate trastuzumab-DM1 for the treatment of human epidermal growth factor receptor 2 (HER2)-positive breast cancer after prior HER2-directed therapy. *J. Clin. Oncol.* **29,** 398–405
5. Ritter, C. A., Perez-Torres, M., Rinehart, C., Guix, M., Dugger, T., Engelman, J. A., and Arteaga, C. L. (2007) Human breast cancer cells selected for resistance to trastuzumab in vivo overexpress epidermal growth factor receptor and ErbB ligands and remain dependent on the ErbB receptor network. *Clin. Cancer Res.* **13,** 4909–4919
6. Lu, Y., Zi, X., Zhao, Y., Mascarenhas, D., and Pollak, M. (2001) Insulin-like growth factor-I receptor signaling and resistance to trastuzumab (Herceptin). *J. Natl. Cancer Inst.* **93,** 1852–1857
7. Nahta, R., Yuan, L. X., Zhang, B., Kobayashi, R., and Esteva, F. J. (2005) Insulin-like growth factor-I receptor/human epidermal growth factor receptor 2 heterodimerization contributes to trastuzumab resistance of breast cancer cells. *Cancer Res.* **65,** 11118–11128
8. Zhuang, G., Brantley-Sieders, D. M., Vaught, D., Yu, J., Xie, L., Wells, S., Jackson, D., Muraoka-Cook, R., Arteaga, C., and Chen, J. (2010) Elevation of receptor tyrosine kinase EphA2 mediates resistance to trastuzumab therapy. *Cancer Res.* **70,** 299–308
9. Garrett, J. T., Olivares, M. G., Rinehart, C., Granja-Ingram, N. D., Sanchez, V., Chakrabarty, A., Dave, B., Cook, R. S., Pao, W., McKinely, E., Manning, H. C., Chang, J., and Arteaga, C. L. (2011) Transcriptional and posttranslational up-regulation of HER3 (ErbB3) compensates for inhibition of the HER2 tyrosine kinase. *Proc. Natl. Acad. Sci. U.S.A.* **108,** 5021–5026
10. Liang, K., Esteva, F. J., Albarracin, C., Stemke-Hale, K., Lu, Y., Bianchini, G., Yang, C. Y., Li, Y., Li, X., Chen, C. T., Mills, G. B., Hortobagyi, G. N., Mendelsohn, J., Hung, M. C., and Fan, Z. (2010) Recombinant human erythropoietin antagonizes trastuzumab treatment of breast cancer cells via Jak2-mediated Src activation and PTEN inactivation. *Cancer Cell* **18,** 423–435
11. Zhang, S., Huang, W. C., Li, P., Guo, H., Poh, S. B., Brady, S. W., Xiong, Y., Tseng, L. M., Li, S. H., Ding, Z., Sahin, A. A., Esteva, F. J., Hortobagyi, G. N., and Yu, D. (2011) Combating trastuzumab resistance by targeting SRC, a common node downstream of multiple resistance pathways. *Nat. Med.* **17,** 461–469
12. Mukohara, T. (2011) Mechanisms of resistance to anti-human epidermal growth factor receptor 2 agents in breast cancer. *Cancer Sci.* **102,** 1–8
13. Berns, K., Horlings, H. M., Hennessy, B. T., Madiredjo, M., Hijmans, E. M., Beelen, K., Linn, S. C., Gonzalez-Angulo, A. M., Stemke-Hale, K., Hauptmann, M., Beijersbergen, R. L., Mills, G. B., van de Vijver, M. J., and Bernards, R. (2007) A functional genetic approach identifies the PI3K pathway as a major determinant of trastuzumab resistance in breast cancer. *Cancer Cell* **12,** 395–402
14. Scaltriti, M., Eichhorn, P. J., Cortes, J., Prudkin, L., Aura, C., Jimenez, J., Chandarlapaty, S., Serra, V., Prat, A., Ibrahim, Y. H., Guzman, M., Gili, M., Rodriguez, O., Rodriguez, S., Perez, J., Green, S. R., Mai, S., Rosen, N., Hudis, C., and Baselga, J. (2011) Cyclin E amplification/overexpression is a mechanism of trastuzumab resistance in HER2+ breast cancer patients. *Proc. Natl. Acad. Sci. U.S.A.* **108,** 3761–3766
15. Arribas, J., Baselga, J., Pedersen, K., and Parra-Palau, J. L. (2011) p95HER2 and breast cancer. *Cancer Res.* **71,** 1515–1519
16. Scaltriti, M., Rojo, F., Ocana, A., Anido, J., Guzman, M., Cortes, J., Di Cosimo, S., Matias-Guiu, X., Ramon y Cajal, S., Arribas, J., and Baselga, J. (2007) Expression of p95HER2, a truncated form of the HER2 receptor, and response to anti-HER2 therapies in breast cancer. *J. Natl. Cancer Inst.* **99,** 628–638
17. Nagy, P., Friedlander, E., Tanner, M., Kapanen, A. I., Carraway, K. L., Isola, J., and Jovin, T. M. (2005) Decreased accessibility and lack of activation of ErbB2 in JIMT-1, a herceptin-resistant, MUC4-expressing breast cancer cell line. *Cancer Res.* **65,** 473–482
18. Price-Schiavi, S. A., Jepson, S., Li, P., Arango, M., Rudland, P. S., Yee, L., and Carraway, K. L. (2002) Rat MUC4 (sialomucin complex) reduces binding of anti-ErbB2 antibodies to tumor cell surfaces, a potential mechanism for herceptin resistance. *Int. J. Cancer* **99,** 783–791
19. Olsen, J. V., Blagoev, B., Gnad, F., Macek, B., Kumar, C., Mortensen, P., and Mann, M. (2006) Global, in vivo, and site-specific phosphorylation dynamics in signaling networks. *Cell* **127,** 635–648
20. Blagoev, B., Ong, S. E., Kratchmarova, I., and Mann, M. (2004) Temporal analysis of phosphotyrosine-dependent signaling networks by quantitative proteomics. *Nat. Biotechnol.* **22,** 1139–1145
21. Kratchmarova, I., Blagoev, B., Haack-Sorensen, M., Kassem, M., and Mann, M. (2005) Mechanism of divergent growth factor effects in mesenchymal stem cell differentiation. *Science* **308,** 1472–1477
22. Wolf-Yadlin, A., Kumar, N., Zhang, Y., Hautaniemi, S., Zaman, M., Kim, H. D., Grantcharova, V., Lauffenburger, D. A., and White, F. M. (2006)

Effects of HER2 overexpression on cell signaling networks governing proliferation and migration. *Mol. Syst. Biol.* **2,** 54
23. Kumar, N., Wolf-Yadlin, A., White, F. M., and Lauffenburger, D. A. (2007) Modeling HER2 effects on cell behavior from mass spectrometry phosphotyrosine data. *PLoS Comput. Biol.* **3,** e4
24. Bose, R., Molina, H., Patterson, A. S., Bitok, J. K., Periaswamy, B., Bader, J. S., Pandey, A., and Cole, P. A. (2006) Phosphoproteomic analysis of Her2/neu signaling and inhibition. *Proc. Natl. Acad. Sci. U.S.A.* **103,** 9773–9778
25. Mukherji, M., Brill, L. M., Ficarro, S. B., Hampton, G. M., and Schultz, P. G. (2006) A phosphoproteomic analysis of the ErbB2 receptor tyrosine kinase signaling pathways. *Biochemistry* **45,** 15529–15540
26. Zhang, G., Fenyo, D., and Neubert, T. A. (2008) Screening for EphB signaling effectors using SILAC with a linear ion trap-orbitrap mass spectrometer. *J. Proteome Res.* **7,** 4715–4726
27. Zhang, G., Spellman, D. S., Skolnik, E. Y., and Neubert, T. A. (2006) Quantitative phosphotyrosine proteomics of EphB2 signaling by stable isotope labeling with amino acids in cell culture (SILAC). *J. Proteome Res.* **5,** 581–588
28. Jorgensen, C., Sherman, A., Chen, G. I., Pasculescu, A., Poliakov, A., Hsiung, M., Larsen, B., Wilkinson, D. G., Linding, R., and Pawson, T. (2009) Cell-specific information processing in segregating populations of Eph receptor ephrin-expressing cells. *Science* **326,** 1502–1509
29. Kruger, M., Kratchmarova, I., Blagoev, B., Tseng, Y. H., Kahn, C. R., and Mann, M. (2008) Dissection of the insulin signaling pathway via quantitative phosphoproteomics. *Proc. Natl. Acad. Sci. U.S.A.* **105,** 2451–2456
30. Schmelzle, K., Kane, S., Gridley, S., Lienhard, G. E., and White, F. M. (2006) Temporal dynamics of tyrosine phosphorylation in insulin signaling. *Diabetes* **55,** 2171–2179
31. Hammond, D. E., Hyde, R., Kratchmarova, I., Beynon, R. J., Blagoev, B., and Clague, M. J. (2010) Quantitative analysis of HGF and EGF-dependent phosphotyrosine signaling networks. *J Proteome Res.* **9**, 2734–2742
32. Konecny, G. E., Pegram, M. D., Venkatesan, N., Finn, R., Yang, G., Rahmeh, M., Untch, M., Rusnak, D. W., Spehar, G., Mullin, R. J., Keith, B. R., Gilmer, T. M., Berger, M., Podratz, K. C., and Slamon, D. J. (2006) Activity of the dual kinase inhibitor lapatinib (GW572016) against HER-2-overexpressing and trastuzumab-treated breast cancer cells. *Cancer Res.* **66,** 1630–1639
33. Hu, X., Stern, H. M., Ge, L., O'Brien, C., Haydu, L., Honchell, C. D., Haverty, P. M., Peters, B. A., Wu, T. D., Amler, L. C., Chant, J., Stokoe, D., Lackner, M. R., and Cavet, G. (2009) Genetic alterations and oncogenic pathways associated with breast cancer subtypes. *Mol. Cancer Res.* **7,** 511–522
34. Pimienta, G., Chaerkady, R., and Pandey, A. (2009) SILAC for global phosphoproteomic analysis. *Methods Mol. Biol.* **527**, 107–116, x
35. Pinske, M. W. H., Uitto, P. M., Hilhorst, M. J., Ooms, B., and Heck, A. J. R. (2006) Selective isolation at the femtomole level of phosphopeptides from proteolytic digests using 2D-nanoLC-ESI-MS/MS and titanium dioxide precolumns. *Anal. Chem.* **76,** 3935–3943
36. Larsen, M. R., Thingholm, T. E., Jensen, O. N., Roepstorff, P., and Jorgenson, T. J. D. (2005) Highly selective enrichment of phosphorylated peptides from peptide mixtures using titanium dioxide microcolumns. *Mol. Cell. Proteomics* **4,** 873–886
37. Thingholm, T. E., Jorgensen, T. J. D., Jensen, O. N., and Larsen, M. R. (2006) Highly selective enrichment of phosphorylated peptides using titanium dioxide. *Nat. Protoc.* **1,** 1929–1935
38. Syka, J. E. P., Marto, J. A., Bai, D. L., Horning, S., Senko, M. W., Schwartz, J. C., Ueberheide, B., Gacia, B., Busby, S., Muratore, T., Shabanowitz, J., and Hunt, D. F. (2004) Novel linear quadrupole ion trap/FT mass spectrometer: performance characterization and use in the comparative analysis of histone H3 post-translational modifications. *J. Proteome Res.* **3,** 621–626
39. Cox, J., and Mann, M. (2008) MaxQuant enables high peptide identification rates, individualized p.p.b.-range mass accuracies and proteome-wide quantification. *Nat. Biotechnol.* **26,** 1367–1372
40. Cox, J., Neuhauser, N., Michalski, A., Scheltema, R. A., Olsen, J. V., and Mann, M. (2011) Andromeda: a peptide search engine integrated into the MaxQuant environment. *J. Proteome Res.* **10**, 1794–1805
41. Thomas, P. D., Campbell, M. J., Kejariwal, A., Mi, H., Karlak, B., Daverman, R., Diemer, K., Muruganujan, A., and Narechania, A. (2003) PANTHER: a library of protein families and subfamilies indexed by function. *Genome Res.* **13,** 2129–2141
42. Thomas, P. D., Kejariwal, A., Guo, N., Mi, H., Campbell, M. J., Muruganujan, A., and Lazareva-Ulitsky, B. (2006) Applications for protein sequence-function evolution data: mRNA/protein expression analysis and coding SNP scoring tools. *Nucleic Acids Res.* **34,** W645–W650
43. Page, B., Page, M., and Noel, C. (1993) A new fluorometric assay for cytotoxicity measurements in-vitro. *Int. J. Oncol.* **3,** 473–476
44. Ong, S. E., Blagoev, B., Kratchmarova, I., Kristensen, D. B., Steen, H., Pandey, A., and Mann, M. (2002) Stable isotope labeling by amino acids in cell culture, SILAC, as a simple and accurate approach to expression proteomics. *Mol. Cell. Proteomics* **1,** 376–386
45. Pinkse, M. W., Mohammed, S., Gouw, J. W., van Breukelen, B., Vos, H. R., and Heck, A. J. (2008) Highly robust, automated, and sensitive online TiO2-based phosphoproteomics applied to study endogenous phosphorylation in Drosophila melanogaster. *J. Proteome Res.* **7,** 687–697
46. Kao, J., Salari, K., Bocanegra, M., Choi, Y. L., Girard, L., Gandhi, J., Kwei, K. A., Hernandez-Boussard, T., Wang, P., Gazdar, A. F., Minna, J. D., and Pollack, J. R. (2009) Molecular profiling of breast cancer cell lines defines relevant tumor models and provides a resource for cancer gene discovery. *PLoS One* **4,** e6146
47. Liu, H., Ong, S. E., Badu-Nkansah, K., Schindler, J., White, F. M., and Hynes, R. O. (2011) CUB-domain-containing protein 1 (CDCP1) activates Src to promote melanoma metastasis. *Proc. Natl. Acad. Sci. U.S.A.* **108,** 1379–1384
48. Razorenova, O. V., Finger, E. C., Colavitti, R., Chernikova, S. B., Boiko, A. D., Chan, C. K., Krieg, A., Bedogni, B., LaGory, E., Weissman, I. L., Broome-Powell, M., and Giaccia, A. J. (2011) VHL loss in renal cell carcinoma leads to up-regulation of CUB domain-containing protein 1 to stimulate PKC{delta}-driven migration. *Proc. Natl. Acad. Sci. U.S.A.* **108,** 1931–1936
49. Spassov, D. S., Wong, C. H., Sergina, N., Ahuja, D., Fried, M., Sheppard, D., and Moasser, M. M. (2011) Phosphorylation of Trask by Src kinases inhibits integrin clustering and functions in exclusion with focal adhesion signaling. *Mol. Cell. Biol.* **31,** 766–782
50. Guan, J. L. (1997) Role of focal adhesion kinase in integrin signaling. *Int. J. Biochem. Cell Biol.* **29,** 1085–1096
51. Mitra, S. K., and Schlaepfer, D. D. (2006) Integrin-regulated FAK-Src signaling in normal and cancer cells. *Curr. Opin. Cell Biol.* **18,** 516–523
52. Thelemann, A., Petti, F., Griffin, G., Iwata, K., Hunt, T., Settinari, T., Fenyo, D., Gibson, N., and Haley, J. D. (2005) Phosphotyrosine signaling networks in epidermal growth factor receptor overexpressing squamous carcinoma cells. *Mol. Cell. Proteomics* **4,** 356–376
53. Ucar, D. A., Dang, L. H., and Hochwald, S. N. (2011) Focal adhesion kinase signaling and function in pancreatic cancer. *Front. Biosci. (Elite Ed.)* **3,** 750–756
54. Zhao, X., and Guan, J. L. (2011) Focal adhesion kinase and its signaling pathways in cell migration and angiogenesis. *Adv. Drug Deliv. Rev.* **63,** 610–615
55. Surawska, H., Ma, P. C., and Salgia, R. (2004) The role of ephrins and Eph receptors in cancer. *Cytokine Growth Factor Rev.* **15,** 419–433
56. Korpal, M., and Kang, Y. Targeting the transforming growth factor-beta signalling pathway in metastatic cancer. *Eur. J. Cancer* **46**, 1232–1240
57. Schniewind, B., Groth, S., Sebens Muerkoster, S., Sipos, B., Schafer, H., Kalthoff, H., Fandrich, F., and Ungefroren, H. (2007) Dissecting the role of TGF-beta type I receptor/ALK5 in pancreatic ductal adenocarcinoma: Smad activation is crucial for both the tumor suppressive and prometastatic function. *Oncogene* **26,** 4850–4862
58. Siegel, P. M., Shu, W., Cardiff, R. D., Muller, W. J., and Massague, J. (2003) Transforming growth factor beta signaling impairs Neu-induced mammary tumorigenesis while promoting pulmonary metastasis. *Proc. Natl. Acad. Sci. U.S.A.* **100,** 8430–8435
59. Zheng, W. (2009) Genetic polymorphisms in the transforming growth factor-beta signaling pathways and breast cancer risk and survival. *Methods Mol. Biol.* **472,** 265–277
60. Xia, X., Cheng, A., Lessor, T., Zhang, Y., and Hamburger, A. W. (2001) Ebp1, an ErbB-3 binding protein, interacts with Rb and affects Rb transcriptional regulation. *J. Cell. Physiol.* **187,** 209–217
61. Zhang, Y., Woodford, N., Xia, X., and Hamburger, A. W. (2003) Repression of E2F1-mediated transcription by the ErbB3 binding protein Ebp1 involves histone deacetylases. *Nucleic Acids Res.* **31,** 2168–2177
62. Li, Y., Dong, X., Yin, Y., Su, Y., Xu, Q., Zhang, Y., Pang, X., and Chen, W.

(2005) BJ-TSA-9, a novel human tumor-specific gene, has potential as a biomarker of lung cancer. *Neoplasia* **7,** 1073–1080
63. Liu, L., Liao, G. Q., He, P., Zhu, H., Liu, P. H., Qu, Y. M., Song, X. M., Xu, Q. W., Gao, Q., Zhang, Y., Chen, W. F., and Yin, Y. H. (2008) Detection of circulating cancer cells in lung cancer patients with a panel of marker genes. *Biochem. Biophys. Res. Commun.* **372,** 756–760
64. Du, Q., Zhang, Y., Tian, X. X., Li, Y., and Fang, W. G. (2009) MAGE-D1 inhibits proliferation, migration and invasion of human breast cancer cells. *Oncol. Rep.* **22,** 659–665
65. Kobayashi, D., Kumagai, J., Morikawa, T., Wilson-Morifuji, M., Wilson, A., Irie, A., and Araki, N. (2009) An integrated approach of differential mass spectrometry and gene ontology analysis identified novel proteins regulating neuronal differentiation and survival. *Mol. Cell. Proteomics* **8,** 2350–2367
66. Chapman, M. A., Lawrence, M. S., Keats, J. J., Cibulskis, K., Sougnez, C., Schinzel, A. C., Harview, C. L., Brunet, J. P., Ahmann, G. J., Adli, M., Anderson, K. C., Ardlie, K. G., Auclair, D., Baker, A., Bergsagel, P. L., Bernstein, B. E., Drier, Y., Fonseca, R., Gabriel, S. B., Hofmeister, C. C., Jagannath, S., Jakubowiak, A. J., Krishnan, A., Levy, J., Liefeld, T., Lonial, S., Mahan, S., Mfuko, B., Monti, S., Perkins, L. M., Onofrio, R., Pugh, T. J., Rajkumar, S. V., Ramos, A. H., Siegel, D. S., Sivachenko, A., Stewart, A. K., Trudel, S., Vij, R., Voet, D., Winckler, W., Zimmerman, T., Carpten, J., Trent, J., Hahn, W. C., Garraway, L. A., Meyerson, M., Lander, E. S., Getz, G., and Golub, T. R. (2011) Initial genome sequencing and analysis of multiple myeloma. *Nature* **471**, 467–472
67. Sundvall, M., Iljin, K., Kilpinen, S., Sara, H., Kallioniemi, O. P., and Elenius, K. (2008) Role of ErbB4 in breast cancer. *J. Mammary Gland Biol. Neoplasia* **13,** 259–268
68. Muraoka-Cook, R. S., Feng, S. M., Strunk, K. E., and Earp, H. S., 3rd (2008) ErbB4/HER4: role in mammary gland development, differentiation and growth inhibition. *J. Mammary Gland Biol. Neoplasia* **13**, 235–246
69. Suo, Z., Risberg, B., Kalsson, M. G., Willman, K., Tierens, A., Skovlund, E., and Nesland, J. M. (2002) EGFR family expression in breast carcinomas. c-erbB-2 and c-erbB-4 receptors have different effects on survival. *J. Pathol.* **196,** 17–25
70. Barnes, N. L., Khavari, S., Boland, G. P., Cramer, A., Knox, W. F., and Bundred, N. J. (2005) Absence of HER4 expression predicts recurrence of ductal carcinoma in situ of the breast. *Clin. Cancer Res.* **11,** 2163–2168